J Mater Sci: Mater Electron (2017) 28:11969–11978
DOI 10.1007/s10854-017-7006-3

A study of microwave absorbing properties in Co–Gd doped M-type Ba–Sr hexaferrites prepared using ceramic method

Rajat Joshi[1] · Charanjeet Singh[1,3] · Jasbir Singh[2] · Dalveer Kaur[4] · S. Bindra Narang[3] · Rajshree B. Jotania[5]

Received: 19 September 2016 / Accepted: 21 April 2017 / Published online: 2 May 2017

Abstract M-type Barium-Stronium hexaferrites with the chemical composition $Ba_{0.5}Sr_{0.5}Co_xGd_xFe_{12-2x}O_{19}$ (x = 0.0, 0.2, 0.4, 0.6, 0.8 and 1.0) were prepared using a conventional ceramic method. X-ray diffraction (XRD) technique was used to explore the structure characterization and phase purity of the prepared compositions. The absorber testing device method was adopted for investigating the dependence of microwave absorption of ferrite compositions on substitution and thickness from 8.2 to 12.4 GHz. The quarter wavelength and impedance matching mechanism are explored to evaluate the microwave absorption. XRD analysis revealed formation of M (magnetoplumblite) phase in compositions x = 0.0, 0.2, while doped compositions (x = 0.4, 0.6, 0.8 and 1.0) displayed coexistence of M-phase along with orthorhombic phase ($BaFe_2O_4$). For maximum microwave absorption, the doping of Co^{2+} and Gd^{3+} leads to the reduction in thickness of composition and frequency shift from the high to low frequency region. Composition x = 0.8 exhibits good microwave absorber characteristics with 96.90% absorbed power and reflection loss of −15.0 dB at matching frequency and thickness of 8.2 GHz and 2.9 mm respectively.

✉ Charanjeet Singh
charanjeet2003@rediffmail.com

[1] Department of Electronics and Communication Engineering, Rayat Bahra Institute of Engineering and Nanotechnology Hoshiarpur, Hoshiarpur, Punjab, India

[2] Department of Electronics and Communication Engineering, Yadavindra college of Engineering, Punjabi University Guru Kashi Campus, Talwandi Sabo, Punjab, India

[3] Department of Electronics Technology, Guru Nanak Dev University, Amritsar, Punjab, India

[4] Department of Electronics and Communication Engineering, I.K.G. Punjab Technical University, Kapurthla, India

[5] Department of Physics, University school of sciences, Gujarat University, Navrangpura, Ahmedabad, Gujrat 380009, India

1 Introduction

The increase in number and type of giga hertz (GHz) electronic devices, Wi-Fi, Wi-MAX technology, mobile phone communication, military and aerospace applications, wireless local/wide/metro area networks (LAN, WAN or MAN) has pumped up the atmosphere with the electromagnetic interference (EMI) or wireless pollution. The EMI induces undesired spurious fields through the medium, for example, electrical or electronic devices, it passes through causing the malfunctioning of devices. This has motivated the researchers to explore the materials, to combat EMI, in the form of microwave absorbers or radar absorbing materials (RAM), anti-electromagnetic interference coatings and electromagnetic interference (EMI) suppressors.

M-type hexagonal ferrites are ferrimagnetic oxides having high electrical resistance, good chemical stability and corrosion resistivity, low density, low cost of synthesis etc. and are utilized specifically as microwave absorber attributing to their large dielectric and/or magnetic losses in GHz region, [1–3]. Apart from this, these ferrites are incorporated in disk drivers, video recorders, channel filter in telecommunication, gyromagnetic microwave devices, high power transmitters, digital switching applications etc. [4, 5]. M-type hexaferrites have gained more attention compared to other class of ferrites (W, X, Y, U and Z) because of their greater structural stability and unique magnetoplumbite nature. The literature survey shows that lots of work carried out in order to investigate magnetic

and dielectric properties of doped and undoped Sr^{2+}, Ca^{2+}, Pb^{2+}, Ba^{2+} and La^{3+} as alkali earth metal cations [6–10].

Sombra et al. studied magnetic and dielectric properties of M-type barium strontium ferrites in RF and Microwave frequency range [11]; where as K. K. Mallick [12] has investigated magnetic and structural properties of M-type barium hexaferrite prepared by co-precipitation and Deniela et al. [13] worked on the effect of rare-earth ions addition on phase formation and magnetic properties of $Sr_{1-x}Ln_xFe_{12}O_{19}$ (Ln = Pr, Nd, Sm, Eu and Gd) hexaferrites.

A perusal of reports are available on microwave absorption in ferrites: Kameli et al. [14] investigated cerium doped M-type $Ba_{1-x}Ce_xFe_{12}O_{19}$ hexagonal ferrites and observed maximum reflection loss −16.43 dB in X-Band at 10.3 GHz. Jafarian et al. [15] studied M-type $BaMg_xZn_xX_{2x}Fe_{12-4x}O_{19}$ (x = Zr, Ce, Sn) hexagonal ferrites and found maximum reflection loss of -19.3 dB at 12.3 GHz with 1.7 GHz bandwidth in $BaMg_{0.9}Zn_{0.9}Zr_{1.8}Fe_{8.4}O_{19}$ ferrite. Moradi et al. [16] prepared M-type $BaMg_{x/2}Mn_{x/2}Co_xTi_{2x}Fe_{12-4x}O_{19}$ hexaferrites and concluded with maximum reflection loss of ~ −17 dB in x = 0.5 around 10 GHz at the matching thickness of 2.7 mm.

In this manuscript, we are reporting structural and microwave absorption characteristics of Co-Gd doped $Ba_{0.5}Sr_{0.5}Co_xGd_xFe_{12-2x}O_{19}$ (x = 0.0, 0.2, 0.4, 0.6, 0.8 and 1.0) hexagonal ferrites prepared by a ceramic method and sintered at 1150 °C for 15 h. The microwave absorption has been evaluated by quarter wavelength mechanism and impedance matching mechanism, which to the authors' best knowledge is not reported yet.

2 Experimental procedure

2.1 Preparation of cobalt–gadolinium doped barium–strontium hexaferrites

A series of polycrystalline hexaferrites with chemical composition $Ba_{0.5}Sr_{0.5}Co_xGd_xFe_{12-2x}O_{19}$ (x = 0.0, 0.2, 0.4, 0.6, 0.8 and 1.0) was prepared using a conventional ceramic method [17]. A high purity of metal carbonates and oxides $BaCo_3$ (AR grade-Sigma Aldrich, 99.98% pure), $SrCo_3$ (AR grade-Sigma Aldrich, 99.98% pure), $CoCO_3$ (AR grade-Sigma Aldrich, 99.98% pure), Gd_2O_3 (AR grade-Sigma Aldrich, 99.98% pure) and Fe_2O_3 (AR grade-Sigma Aldrich, 99.98% pure) were used as a starting materials. The stoichiometric amount of chemical reagents were grounded well for 8 h in presence of double distilled water medium using an agate mortar and pastel and then the mixed powder was dried on a hot plate at 80 °C for 3 h. The preparation involved two major steps. In the first step; the stoichiometric amount of oxide mixture was preheated at 1000 °C for 10 h in an electric furnace (heating and cooling rate of a furnace set at ±5 °C) and then slowly cooled to room temperature. The pre-heated powder was rigorously grounded and then pressed into disk shaped pellets using a hydraulic press under a uniaxial pressure of 75 KN/m^2. In the second step, the pellets were finally heated at 1150 °C for 15 h and then slowly cooled to room temperature by air to obtain hexagonal powder samples.

The microwave absorption characteristics of $Ba_{0.5}Sr_{0.5}Co_xGd_xFe_{12-2x}O_{19}$ hexaferrites were studied from 8.2 to 12.4 GHz (X-Band) for different levels of doping of Co^{2+} and Gd^{3+} ions and thickness by absorber testing device (ATD) method [18, 19]. Figure 1a, b represents a schematic block diagram of this method.

The prepared samples were characterized at room temperature using FTIR and X-ray diffraction techniques. The FTIR spectra of all sintered samples were recorded on Bruker Tenor 27-FTIR spectrometer in wave number ranges from 1000 to 400 cm^{-1} using KBr pellet method. The phase purity and crystal structure of obtained hexaferrite samples were examined by X-ray diffraction (XRD) technique (Bruker diffractometer Model D8) using Cu-Kα radiation source (λ = 1.5405 Å, 45.0 kV, 50.0 mA) in the range of 2θ = 20°–70° with a step scan of 0.02° min^{-1}.

The frequency synthesizer (HP Model 83751A) generates frequencies from 8.2 to 12.4 GHz at X-Band in the rectangular waveguide with inner dimensions length = 22.86 mm, breadth = 10.16 mm. The isolator allows the unattenuated microwave propagation from synthesizer to the waveguide, directional coupler and ferrite composition, and it attenuates any reflected signal to prevent its reach towards the synthesizer. The directional coupler has one primary input and two secondary output ports. The peripheral assembly (Isolator, waveguide and directional coupler) has model 9000 of NVIS, India. The ferrite composition with metal backed plate was fitted at the secondary output port 2 and the reflected signal from composition was measured by power meter connected to other secondary output port 1. The microwave power meter (Tektronix-Model 3320) was used to measure the different microwave signals and S_{11} parameter was calculated from reflected power at port 1.

The cathode ray oscilloscope was used to display the change in characteristics (amplitude, phase and frequency) of microwave signal after interacting with ferrite compositions.

The reflection loss (RL) can be expressed using the following relation:

$$\mathrm{RL\,(dB)} = 20\log_{10}(|S_{11}|) \quad (1)$$

The reflection loss of −10 dB equals 90% microwave absorbed power. The large RL parameter accompanies more microwave absorption and vice versa.

The reflected power (%) was calculated as:

$$\text{Reflected Power (\%)} = \left(P_r/P_{rw}\right) \times 100 \quad (2)$$

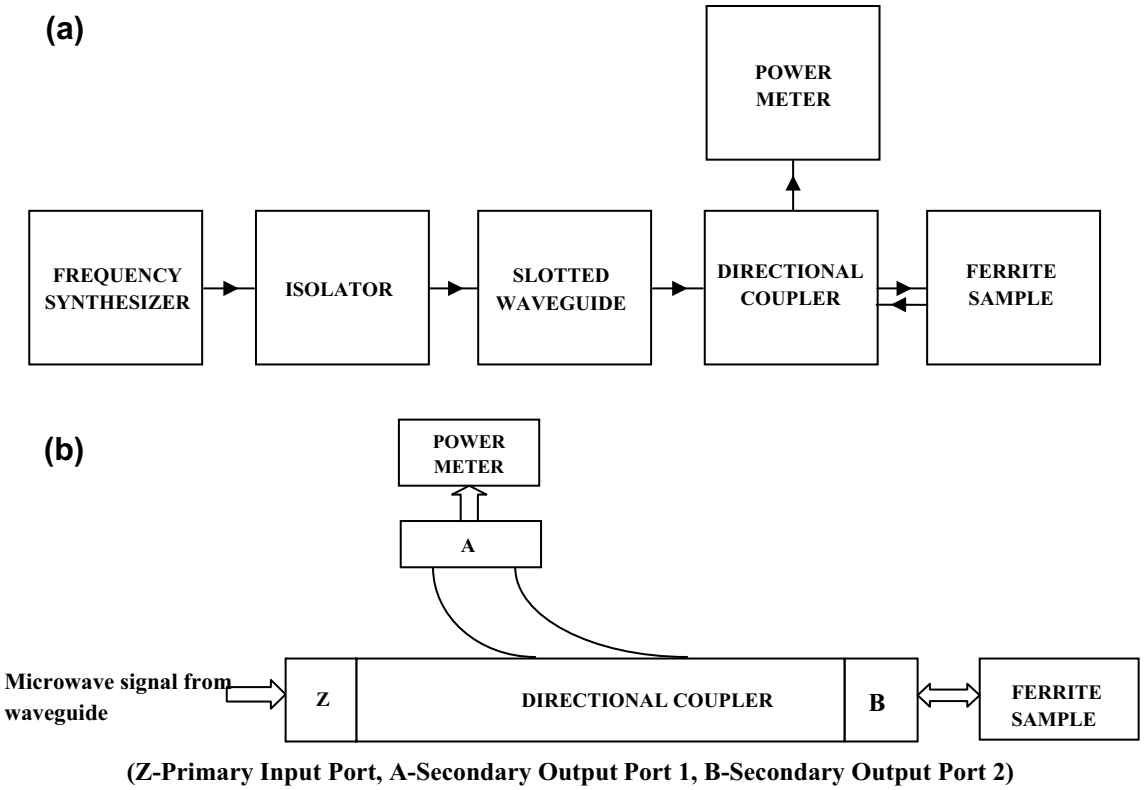

Fig. 1 **a, b** Block diagram of absorber testing device (ATD) method

where P_r was the reflected power from the composition backed by a metal plate and P_{rw} was the reflected power from the metal plate without composition.

The absorbed power was calculated using the following relation:

$$\text{Absorbed Power (\%)} = 100 - \text{Reflected Power (\%)} \quad (3)$$

The selected thickness of the composition corresponding to the optimised microwave absorption are: x = 0.0 (3.0 mm), x = 0.2 (2.8 mm), x = 0.4 (2.9 mm), x = 0.6 (2.8 mm), x = 0.8 (2.9 mm), x = 1.0 (2.6 mm). The terms matching frequency (f_{mat}) and thickness used in the manuscript are associated with maximum absorbed power at a particular frequency and thickness in the composition.

3 Results and discussion

3.1 FTIR analysis

Figure 2 shows FTIR spectra of sintered samples recorded in wave number ranges from 1000 to 400 cm^{-1}. The two absorption bands observed between wave number ranging from 400 to 600 cm^{-1}. The first band near 430 cm^{-1} (ν_2 mode, stretching Fe^{3+}–O^{2-} bond) is attributed to the vibration of ferric ions at octahedral coordination and the second band near 583 cm^{-1} (ν_1 mode, stretching Fe^{3+}–O^{2-} bond) indicates the vibration of ferric ions at the tetrahedral coordination of crystallographic sites [20–24]. These are the common features of all ferrites and confirm the formation of ferrite [25–27].

3.2 XRD analysis

Figure 3a, b shows X-ray powder diffraction patterns of the prepared $Ba_{0.5}Sr_{0.5}Co_xGd_xFe_{(12-2x)}O_{19}$ (x = 0.0, 0.2, 0.4, 0.6, 0.8 and 1.0)hexaferrite samples. The X-ray diffraction patterns were analyzing using 'Powder-X' software. All X-ray diffraction lines were identified with their Müller indices and indexed to magnetoplumbite (M-type) crystal structure with space group $P6_3/mmc$, [JCPDS: 51-1879, a = b = 5.8862 Å, c = 23.137(1) Å]. The XRD analysis of x = 0.0 and x = 0.2 samples show the major mono phase of $Ba_{0.5}Sr_{0.5}Fe_{12}O_{19}$ (hexagonal); while x > 0.2 samples indicate the major phase of $Ba_{0.5}Sr_{0.5}Fe_{12}O_{19}$ (hexagonal) along with the secondary phase of orthorhombic-$BaFe_2O_4$ [space group Pmcn (62), JCPDS: 77-2337, a = 17.34 Å, b = 9.335 Å and c = 10.881 Å]. The similar result was observed in M-type barium hexaferrites reported by Rashad et al. [28].

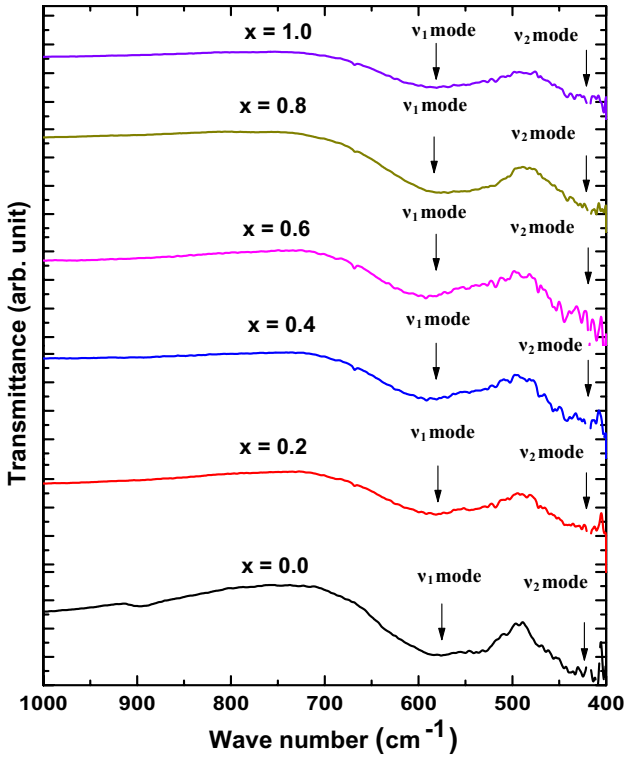

Fig. 2 FTIR spectra of $Ba_{0.5}Sr_{0.5}Co_xGd_xFe_{(12-2x)}O_{19}$ (x = 0.0, 0.2, 0.4, 0.6, 0.8, 1.0) hexaferrites compositions heated at 1150 °C

The lattice parameters ($a = b$ and c) and unit cell volume (V) of all prepared samples were calculated using following equations.

For hexagonal structure $a = b \neq c$ *and* $\alpha = \beta = 90°$ and $\gamma = 120°$

$$\frac{1}{d_{hkl}^2} = \frac{4}{3}\left(\frac{h^2}{a^2} + \frac{hk}{a^2} + \frac{k^2}{a^2}\right) + \frac{l^2}{c^2} \quad (4)$$

$$V = \frac{\sqrt{3}}{2}a^2c \quad (5)$$

where d_{hkl} is the d-spacing of the lines in XRD pattern and h, k, l are the Müller indices.

Lattice constants (a,c), cell volume (V) and phase percentage $Ba_{0.5}Sr_{0.5}Co_xGd_xFe_{12-2x}O_{19}$ (x = 0.0, 0.2, 0.4, 0.6, 0.8 and 1.0) hexagonal ferrite samples are listed in Table 1. The lattice constant values are found in range of $a = b = 5.867$–5.880 Å, which is slightly lower than standard values ($a = b = 5.8862$ Å); $c = 23.119$–23.273 Å; which are higher than the standard value [$c = 23.137(1)$ Å] and cell volume $V = 690.224$–696.035 (Å)^3 for all sintered samples. The c/a values vary from 3.931 to 3.963, which is lower than standard value (3.980) of M-type hexagonal structure [29]. According to Table 1, the values of lattice constant c found to increase more compared to a as Co–Gd doping increases but the cell volume value found to decrease up to x = 0.4 then it is slightly increased.

It is interesting to note that for x = 0.0, the high intense X-ray diffraction line is observed at $2\theta = 34.20°$ with [h, k, l] value [114] but for doped samples high intense lines are observed at $2\theta \sim 32.1°$ with [h, k, l] value [107]. The relative intensity of diffraction line with hkl-114 tends to decrease from x = 0.0 to 0.2 but this line disappeared in x > 0.2, revealing that from x = 0.4 onwards crystal symmetry is affected as an impure phase of

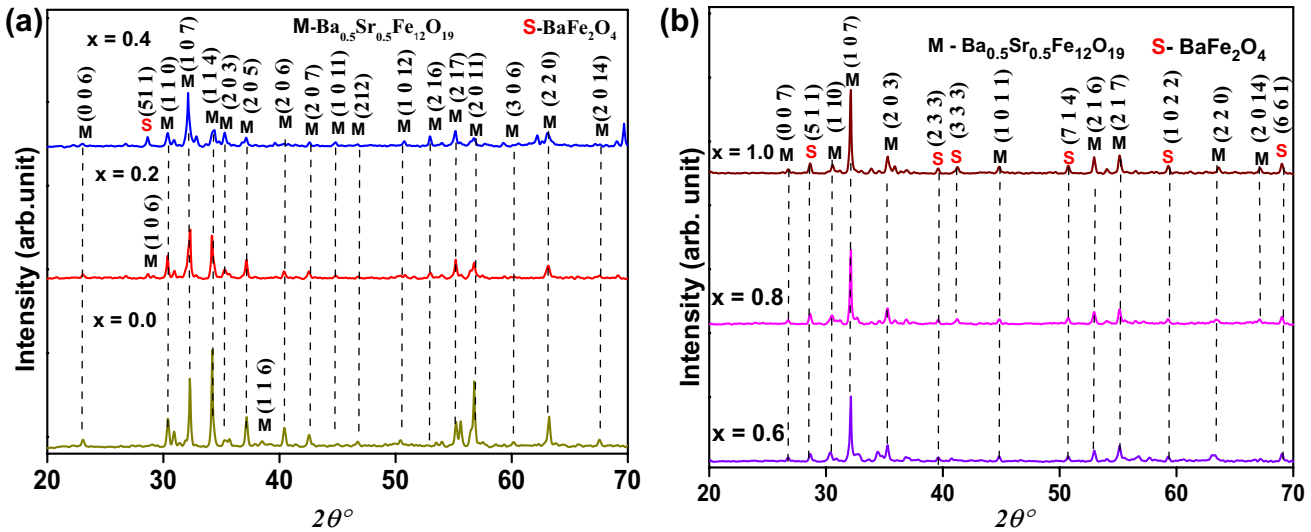

Fig. 3 **a** X-ray diffraction patterns of $Ba_{0.5}Sr_{0.5}Co_xGd_xFe_{(12-2x)}O_{19}$ (x = 0.0, 0.2, 0.4) hexaferrite compositions sintered at 1150 °C for 15 h. **b** X-ray diffraction patterns of $Ba_{0.5}Sr_{0.5}Co_xGd_xFe_{(12-2x)}O_{19}$ (x = 0.6, 0.8, 1.0) hexaferrite compositions sintered at 1150 °C for 15 h

Table 1 Lattice constants, c/a ratio, cell volume, and phase percentage $Ba_{0.5}Sr_{0.5}Co_xGd_xFe_{12-2x}O_{19}$ hexagonal ferrites (x = 0.0, 0.2, 0.4, 0.6, 0.8 and 1.0) sintered at 1150 °C for 15 h

Co–Gd content (x)	2θ (deg.)	Lattice constants		c/a	Cell volume	Percentage of phases	
		a (Å) ± 0.01	c (Å) ± 0.01		V (Å^3) ± 0.01	M (%)	S (%)
0.0	34.240	5.880	23.119	3.931	692.324	100	0
0.2	32.210	5.879	23.120	3.933	692.031	100	0
0.4	32.110	5.878	23.266	3.958	690.244	94.44	5.56
0.6	32.110	5.867	23.228	3.959	692.301	73.33	26.67
0.8	32.116	5.871	23.264	3.963	694.391	75	25
1.0	32.103	5.876	23.273	3.961	696.035	75	25

orthorhombic- BaFe2O4 detected in these samples. It can be also seen from Table 1 that c/a value is increased with doping attributing that the hexagonal crystal symmetry is slightly changed after doping (x > 0.2). The change in crystal symmetry can be correlated with the coexistence of non-magnetic – orthorhombic - BaFe2O4 phase. The percentage of orthorhombic-BaFe2O4 phase is found to minimum (5.56%) in x = 0.4 and maximum (26.67%) in x = 0.6 compositions. The position of diffraction lines of the doped samples is found to shift toward lower angles because of the replacement of the smaller ionic radii Fe^{3+} (0.64 Å) with larger Co^{2+} (0.72 Å) and Gd^{3+} (0.93 Å) cations [30, 31].

3.3 Morphology study

The surface morphology and microstructure analysis of $Ba_{0.5}Sr_{0.5}Co_xGd_xFe_{12-2x}O_{19}$ hexagonal ferrites (x = 0.0, 0.2, 0.4, 0.6, 0.8 and 1.0) sintered at 1150 °C for 15 h were observed by scanning electron microscopy (SEM) and the SEM images of x = 0.0, 0.2, 0.4, 0.6, 0.8 and 1.0 samples are shown in Fig. 4. It can be seen from the images that the formed grains are non-uniform and porosity found to decrease with Co–Gd doping.

3.4 Reflection loss, microwave absorbed power

Figure 5 displays the plots of reflection loss (RL) versus frequency for different doping levels of Co^{2+} and Gd^{3+} ions as well as thickness of compositions in $Ba_{0.5}Sr_{0.5}Co_xGd_xFe_{12-2x}O_{19}$ ferrites (x = 0.0, 0.2, 0.4, 0.6, 0.8 and 1.0). There is an observation of a non-linear decrease in RL parameter encompassing from the low to high frequency region in all ferrite compositions: more dispersion in RL parameter is noted from 8.2 to 10.0 GHz in the prepared compositions. Evidently, all compositions display RL parameter more than −10 dB from 8.2 to 11.3 GHz and thereafter RL parameter is below −10 dB at all frequencies; x = 0.2, 0.8 and 1.0 exhibit their respective maximum RL parameter at 8.2 GHz in the low frequency region. The dopants Co^{2+} and Gd^{3+} lead to an increase or decrease in the amplitude of observed peaks of RL parameter and all compositions owe maximum or minimum values of peaks of RL parameter nearly at the same frequencies along the investigated frequency region.

Figure 6 depicts plots of absorbed power (P_{ab}) versus frequency at different thickness and dopants Co^{2+}–Gd^{3+}. The absorption curves of the compositions get more symmetrical in the high frequency region. The compositions owe >90% absorbed power along the different frequency regions. All doped compositions (x = 0.2, 0.4, 0.6, 0.8 and 1.0) have lowest absorbed power at 11.89 GHz in the high frequency region; x = 1.0 stays at minimum P_{ab} among all compositions. Among all compositions, x = 0.8 stays at large P_{ab} at a number of frequencies along low, middle and high frequency region.

Table 2 shows the variation of maximum absorbed power (P_{amax}) with the corresponding matching frequency (f_{mat}) in different compositions of $Ba_{0.5}Sr_{0.5}Co_xGd_xFe_{12-2x}O_{19}$ ferrites. The doping of Co^{2+} and Gd^{3+} ions reduces the measured thickness for P_{amax} in composition x = 1.0 (2.6 mm) in comparison to undoped composition x = 0.0 (3.0 mm); same behavior is present in x = 0.2, 0.4, 0.6 and 1.0. The dopants shift the P_{amax} from high frequency region in x = 0.0 to low and middle frequency regions in doped compositions: dopants lead to a slight increase in P_{amax} in x = 0.8 and vice-versa in x = 0.2, 0.4, 0.6 and 1.0. Compositions x = 0.2, 0.8 and 1.0 have P_{amax} at 8.2 GHz, while x = 0.0 and 0.6 have at 11.22 and 10.04 GHz respectively.

3.5 Quarter wavelength mechanism

This mechanism [32, 33] enunciates maximum absorption of microwave signal on interaction with material with thickness equals to the quarter wavelength of the microwave signal.

The microwave signal after interaction with metal backed ferrite composition gets partially reflected by ferrite front surface and else will be transmitted through the ferrite. The transmitted signal is reflected by the metal plate behind the ferrite composition and arrives again at the front face of the ferrite. When the reflected signal

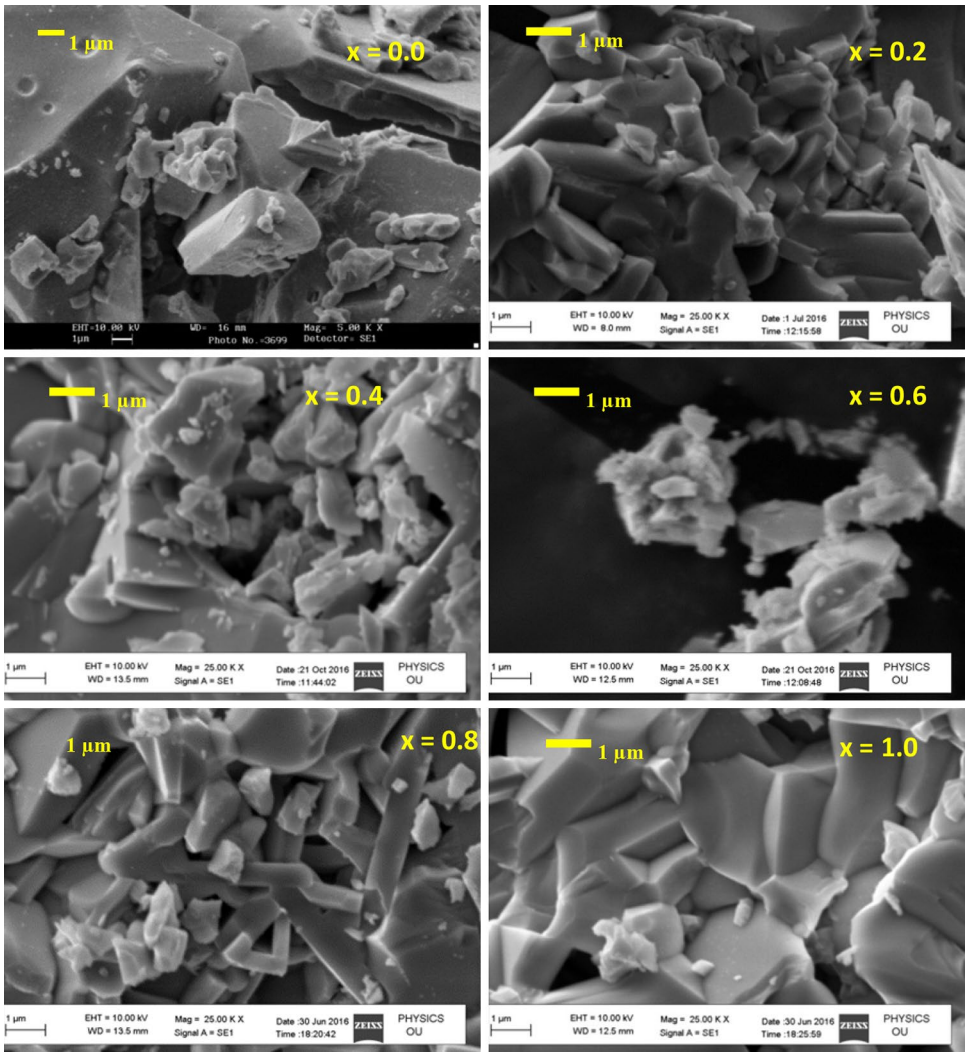

Fig. 4 SEM images of $Ba_{0.5}Sr_{0.5}Co_xGd_xFe_{12-2x}O_{19}$ ferrites (x = 0.0, 0.2, 0.4, 0.6, 0.8 and 1.0) hexaferrite samples sintered at 1150 °C for 15 h

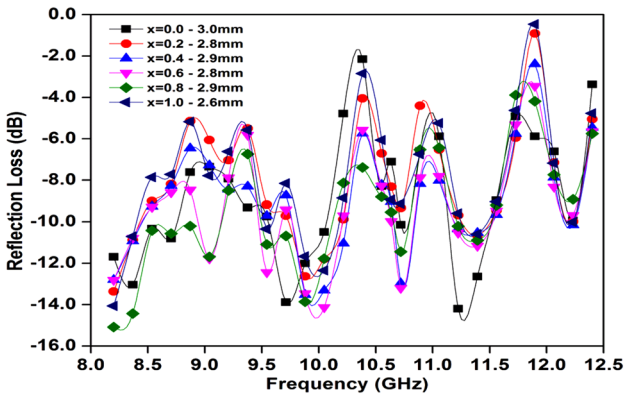

Fig. 5 Plots of reflection loss versus frequency and substitution in $Ba_{0.5}Sr_{0.5}Co_xGd_x\ Fe_{12-2x}O_{19}$ (x = 0.0, 0.2, 0.4, 0.6, 0.8 and 1.0) hexaferrites sintered at 1150 °C for 15 h

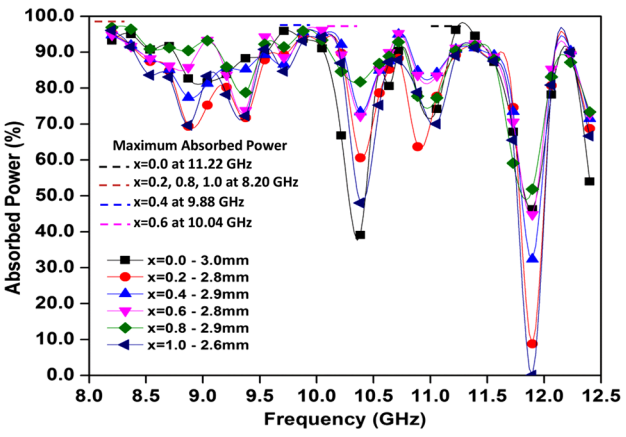

Fig. 6 Plots of absorbed power vs. frequency and substitution in $Ba_{0.5}Sr_{0.5}Co_xGd_xFe_{12-2x}\ O_{19}$ (x = 0.0, 0.2, 0.4, 0.6, 0.8 and 1.0) hexaferrites sintered at 1150 °C for 15 h

Table 2 Maximum absorbed power, matching frequency, measured thickness and calculated thickness in $Ba_{0.5}Sr_{0.5}Co_xGd_xFe_{12-2x}O_{19}$ (x = 0.0, 0.2, 0.4, 0.6, 0.8 and 1.0) hexaferrites sintered at 1150 °C for 15 h

Co–Gd doping (x)	P_{amax} (%)	Matching frequency (f_{mat}) (GHz)	Matching thickness (mm) (measured)	Thickness t = mλ/4 (mm) (calculated) quarter wavelength mechansim
0.0	96.23	11.22	3.0	3.0
0.2	95.39	8.20	2.8	2.4
0.4	95.56	9.88	2.9	3.2
0.6	96.14	10.04	2.8	3.0
0.8	96.90	8.20	2.9	2.6
1.0	96.08	8.20	2.6	2.5

from the front surface of ferrite composition is equal in magnitude and 180° out of phase with the reflected signal from the metal plate, both signals will cancel each other and total reflection will be zero. Thus, this phenomenon can be mathematically represented as:

$$t_m = \frac{n\lambda_0}{4.\sqrt{\mu\varepsilon}}; n = 1, 3, 5 \ldots \ldots . \quad (6)$$

where t_m, λ_0, ε, μ and correspond to thickness, free space wavelength, complex permittivity and complex permeability of the material respectively. The Nicholson-Ross method is used to derive ε and μ from *S*-parameters [34].

Table 2 depicts various parameters associated with quarter wavelength mechanism, for maximum absorbed power, applied in different compositions. The undoped composition x = 0.0 with P_{amax} at 11.22 GHz governs quarter wavelength mechanism; measured thickness is exactly same as calculated thickness (3 mm). The order of contribution of quarter wavelength mechanism in doped compositions is x = 1.0 > x = 0.6 > x = 0.8 > x = 0.4 > x = 0.2: x = 1.0 and 0.6 have calculated thickness approximately same as measured thickness, however, more difference is seen between thoeretical and measured thickness in x = 0.8, 0.4 and 0.2.

Composition x = 0.0, 0.6 and 1.0 with actual or measured thickness 3.0, 2.8 and 2.6 mm are integral multiple of $\lambda_m/4$ (3.0, 3.0 and 2.5 mm) at 11.22, 10.04 and 8.22 respectively. The quarter wavelength mechanism gives more contribution in these compositions than x = 0.2, 0.4 and 0.8, but in spite of that there is not much difference in P_{amax} of these compositions than x = 0.0, 0.6 and 1.0. The next section discusses the reason behind this anomaly.

Table 3 shows −10 dB absorption bandwidth (ABW) shown by compositions; −10 dB bandwidth stands for the band of frequencies for which RL parameter is > −10 dB or absorbed power (P_{ab}) is more than 90%. Composition x = 0.0 and 0.4 exhibit same ABW of 330 MHz from 9.41 to 10.04 and 9.88–10.21 GHz respectively while x = 0.0 and 0.8 have same 500 MHz from 8.20 to 8.70 and 9.54–10.04 GHz. The large ABW of 840 MHz is seen in x = 0.8 among all compositions.

Table 3 −10 dB bandwidth (BW) for RL parameter > −10 dB in $Ba_{0.5}Sr_{0.5}Co_xGd_xFe_{12-2x}O_{19}$ (x = 0.0, 0.4 and x = 0.8) hexaferrites sintered at 1150 °C for 15 h ferrites

Co–Gd doping (x)	Lower frequency f_1 (GHz)	Higher frequency f_2 (GHz)	BW (f_2–f_1) (GHz)
0.0	8.20	8.70	0.50
	9.71	10.04	0.33
0.4	9.88	10.21	0.33
0.8	8.20	9.04	0.84
	9.54	10.04	0.50

3.6 Impedance matching mechanism

The input impedance (Z_{in}) of a single layer absorber can be calculated theoretically on the basis of transmission line theory as [35]:

$$Z_{in} = Z_o\left(\mu_r/\varepsilon_r\right)^{1/2} \tanh\left[j(2\pi ft/c)\left(\mu_r\varepsilon_r\right)^{1/2}\right] \quad (7)$$

where $Z_o = 377\ \Omega$ is the characteristic impedance of free space and ε_r, μ_r, t, f, c denote complex permittivity, complex permeability, thickness, frequency, and velocity of light respectively.

When Z_{in} is equal to Z_o, the condition prevails for infinite absorption of the signal by the composition.

The input impedance in Eq. 7 is of complex nature i.e. $Z_{in} = a + j\ b$, where a is the real part and b is the imaginary part. In an ideal situation when $|Z| = Z_o = 377\ \Omega$ i.e. $Z_{real} = 377\ \Omega$ and $Z_{img} = 0$, the entire signal passing through the material will be absorbed. However, practically $|Z| \neq Z_o = 377\ \Omega$ or $Z_{real} \neq 377\ \Omega$ and/or $Z_{img} \neq 0$, which causes the decrease in absorption. Therefore, absorption decreases when Z_{real} moves farther from 377 Ω and/or Z_{img} is non-zero (positive or negative values).

Figure 7 explains Z_{in}, Z_{real} and Z_{img} values corresponding to the reflection loss or microwave absorption graphs (Figs. 5, 6) observed in compositions. It is evident from the plots that no compositions has $Z_{real} = 377\ \Omega$ and/or $Z_{img} = 0$. However, compositions x = 0.2, 0.4 and 0.8 have

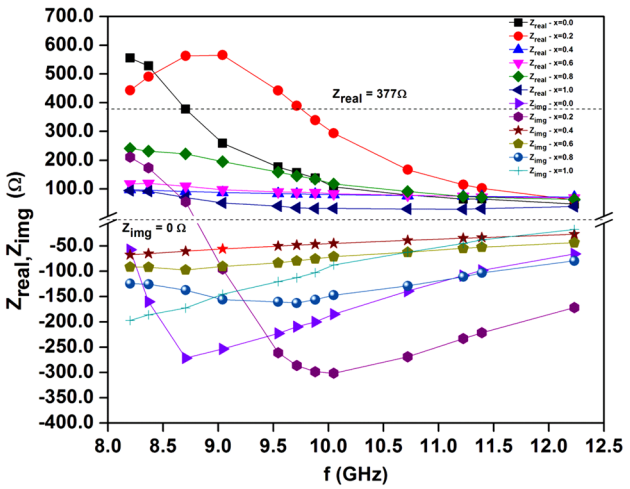

Fig. 7 Impedance matching mechanism with f, Z_{in}, Z_{real} and Z_{img} values corresponding to the peaks in RL parameter in $Ba_{0.5}Sr_{0.5}Co_xGd_xFe_{12-2x}O_{19}$ (x = 0.0, 0.2, 0.4, 0.6, 0.8 and 1.0) hexaferrites sintered at 1150 °C for 15 h ferrites

relatively both Z_{real} and Z_{img} more close to 377 Ω and zero than x = 0.0, 0.6 and 1.0: this gives more contribution of impedance matching mechanism in former compositions. Furthermore the relative contribution in the same compositions can be expressed as x = 0.2 > x = 0.4 > x = 0.8. This gives comparable P_{amax} in x = 0.2, 0.4 and 0.8 with x = 0.0, 0.6 and 1.0 in table Therefore, impedance matching mechanism attributes to the anomaly discussed in the section of quarter wavelength mechanism. Similar variation was reported in Li-Sr-Ni ferrites [36].

The quarter wavelength and impedance matching mechanism enunciate to predict thickness and frequency for maximum microwave absorption and design microwave absorbers.

3.7 Screenshot of microwave signal

Figure 8 displays the screenshots of microwave signal observed on the cathode ray oscilloscope: the two signals are displayed on the snapshots: (i) first signal given to ferrite composition (ii) second signal transmitted from the ferrite composition after passing through it.

The applied frequencies to the compositions on x = 0.0, 0.2, 0.6 and 1.0 are 11.22, 8.20, 10.04 and 8.20 GHz respectively. The spectra in the screenshots convey attenuation (absorption) in the signal after passing through the compositions, and frequency as well as the phase of signal remain unchanged. A similar variation is also seen for other frequencies and, x = 0.4 and 0.8 also exhibit the same behavior.

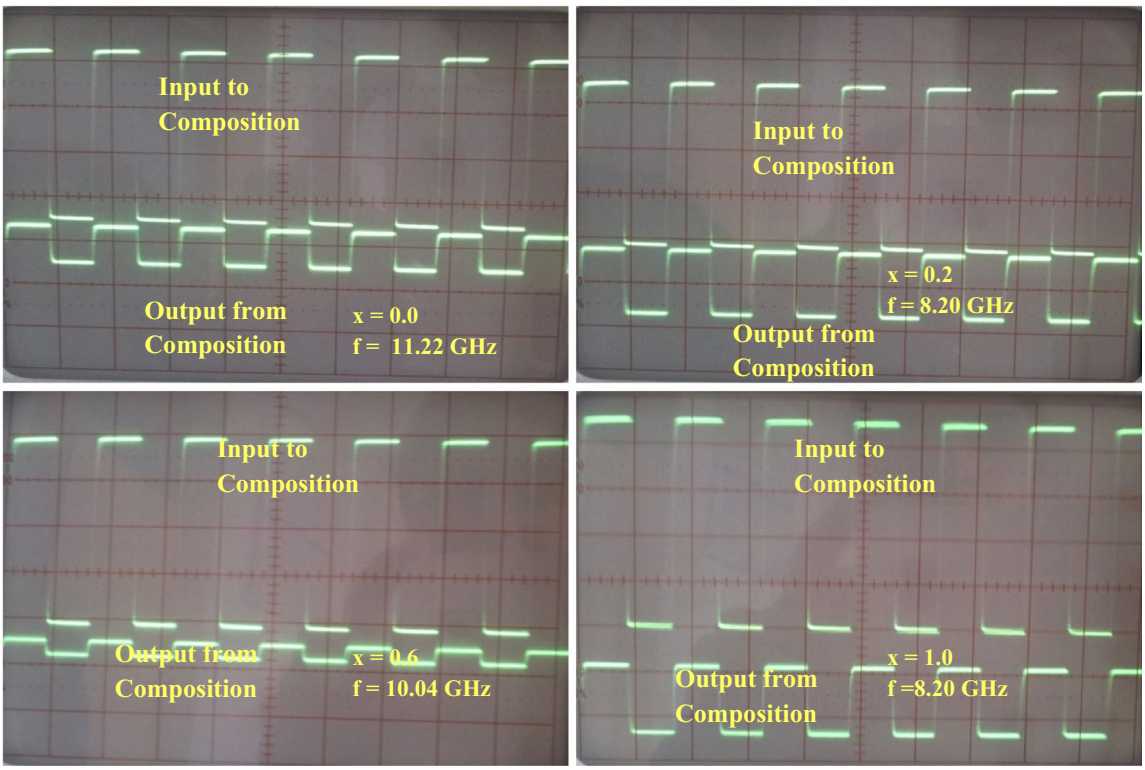

Fig. 8 Screenshots of an input signal and the signal transmitted through the $Ba_{0.5}Sr_{0.5}Co_xGd_xFe_{12-2x}O_{19}$ (x = 0.0, 0.2, 0.6 and 1.0) hexaferrites sintered at 1150 °C for 15 h. (Amplitude value of signal is a guide to the eye)

The ferrite compositions do not alter the frequency and phase of the microwave signal passing through them. In this way, the signal is not distorted, no de-phasing and frequency shift occurs in the microwave signal after interacting with intrinsic fields of ferrite compositions. More specifically, the signal does not suffer from frequency, phase distortion in addition to the intended attenuation.

This variation in signal characteristics is in agreement with that of observed in Figs. 5 and 6: plots on RL parameter and absorbed power displayed only change in amplitude for all compositions with frequency and doping, while no change in phase and frequency of, these two parameters, is seen.

4 Conclusions

$Ba_{0.5}Sr_{0.5}Co_xGd_xFe_{12-2x}O_{19}$ (x = 0.0, 0.2, 0.4, 0.6, 0.8 and 1.0) hexagonal ferrites have been successfully prepared using a ceramic method. The undoped composition x = 0.0 exhibits microwave absorber or EMI reduction characteristics with 96.23% absorbed power at matching frequency and thickness of 11.22 GHz and 3.0 mm respectively. Among doped compositions, x = 0.8 has large 96.90% absorber power at 8.2 GHz and 2.9 mm. The microwave absorption can be tuned by variation of frequency, thickness and dopants.

References

1. I. Ali, M.U. Islam, M.S. Awan, M. Ahmad, M.N. Ashiq, S. Naseem, Effect of Tb^{3+} substitution on the structural and magnetic properties of M-type hexaferrites synthesized by sol–gel auto-combustion technique. J. Alloys Comp. **550**, 564–572 (2013)
2. Z.W. Li, L. Chen, C.K. Ong, Studies of static and high-frequency magnetic properties for M-type ferrite $BaFe_{12-2x}Co_xZr_xO_{19}$. J. Appl. Phys. **92**, 3902–3907 (2002)
3. Y.J. Kim, S.S. Kim, Microwave absorbing properties of Co-substituted Ni/sub 2/W hexaferrites in Ka-band frequencies (26.5–40 GHz). IEEE Trans. Magn. **38**, 3108–3110 (2002)
4. O. Kubo, T. Ido, H. Yokoyama, Properties of Ba ferrite particles for perpendicular magnetic recording media. IEEE Trans. Magn. **18**, 1122–1124 (1982)
5. H. F. Yu, K. C. Huang, Effects of pH and citric acid contents on characteristics of ester-derived $BaFe_{12}O_{19}$ powder. J. Magn. Magn. Mater. **260**, 455–461 (2003)
6. D. Ravinder, P.V.B. Reddy, High-frequency dielectric behaviour of Li–Mg ferrites. Mater. Lett. **57**, 4344–4350 (2003)
7. G. Asghar, M. Anis-ur-Rehman, Structural, dielectric and magnetic properties of Cr–Zn doped strontium hexa-ferrites for high frequency applications. J. Alloys Comp. **526**, 85–90 (2012)
8. F.L. Wei, Magnetic properties of $BaFe_{12-2x}Zn_xZr_xO_{19}$ particles. J. Appl. Phys. **87**(12), 8636–8639 (2000)
9. X. Liu, Research on La^{3+}–Co^{2+}-substituted strontium ferrite magnets for high intrinsic coercive force. J. Magn. Magn. Mater. **305**(2), 524–528 (2006)
10. R.C. Pullar, Hexagonal ferrites: a review of the synthesis, properties and applications of hexaferrite ceramics. Prog. Mater. Sci. **57**(7), 1191–1334 (2012)
11. F.M.M. Pereira, M.R.P. Santos, R.S.T.M. Sohn, J.S. Almeida, A.M.L. Medeiros, M.M. Costa, A.S.B. Sombra, Magnetic and dielectric properties of the M-type barium strontium hexaferrite ($Ba_xSr_{1-x}Fe_{12}O_{19}$) in the RF and microwave (MW) frequency range. J. Mater. Sci. **20**, 408–417 (2009)
12. K.K. Mallick, Magnetic and structural properties of M-type barium hexaferrite prepared by co-precipitation. J. Magn. Magn. Mater. **311**, 683–692 (2007)
13. D. Seifert, J. Töpfer, M. Stadelbauer, R. Grössinger, J.-M. Le Breton, Rare-earth-substituted $Sr1\_xLnxFe_{12}O_{19}$ hexagonal ferrites. J. Am. Ceram. Soc. **94**(7), 2109–2118 (2011)
14. Z. Mosleh, P. Kameli, A. Poorbaferani, M. Ranjbar, H. Salamati, Structural, magnetic and microwave absorption properties of Ce-doped barium hexaferrite. J. Magn. Magn. Mater. **397**, 101–107 (2016)
15. S.S.S. Afghahi, M. Jafarian, Y. Atassi, Microstructural and magnetic studies on $BaMg_xZn_xX_{2x}Fe_{12-4x}O_{19}$ (x = Zr,Ce,Sn) prepared via mechanical activation method to act as a microwave absorber in X-band. J. Magn. Magn. Mater. **406**, 184–191 (2006)
16. R.S. Alam, M. Moradi, H. Nikmanesh, J. Ventura, M. Rostami, Magnetic and microwave absorption properties of $BaMg_{x/2}Mn_{x/2}Co_xTi_{2x}Fe_{12-4x}O_{19}$ hexaferrite nanoparticles. J. Magn. Magn. Mater. **402**, 20–27 (2016)
17. C. Singh, S.B. Narang, I.S. Hudiara, Y. Bai, K. Marina, Hysteresis analysis of Co–Ti substituted M-type Ba–Sr hexagonal ferrite. Mater. Lett. **63**, 1991–1994 (2009)
18. M.R. Meshram, N.K. Agrawal, B. Sinha, P.S. Misra, Characterization of M-type barium hexagonal ferrite-based wide band microwave absorber. J. Magn. Magn. Mater. **271**, 2007–2014 (2004)
19. P. Singh, V.K. Babbar, A. Razdan, R.K. Puri, T.C. Goel, Complex permittivity, permeability, and X-band microwave absorption of CaCoTi ferrite composites. J. Appl. Phys. **87**, 4362–4366 (2000)
20. F.M.M. Pereria, C.A.R. Junior, M.R.P. Santosh, R.S.T.M. Sohn, F.N.A. Freire, J.M. Sasaki, J.A.C. De-Paiva, A.B.S. Sombra, Sructural and dielectric spectroscopic studies of M-type barium hexaferrite alloys ($Ba_xSr_{1-x}Fe_{12}O_{19}$). J. Mater. Sci. **19**, 627–638 (2008)
21. F. Song, X. Shen, J. Xiang, H. Song, Formation and magnetic properties of M–Sr ferrite hollow fibers via organic gel-precursor transformation process. Mater. Chem. Phys. **120**, 213–216 (2010)
22. P.N. Vasambekar, C.B. Kolekar, A.S. Vaigankar, Electrical switching in $Cd_xCo_{1-x}Fe_{2-y}CryO_4$ system. Mater. Res. Bull. **34**, 863–868 (1999)
23. R.S. Patil, S.V. Kakatkar, A.M. Sankpal, S. R. Sawant, S.S. Suryavanshi, U.R. Ghodke, K. Kamat, Infrared absorption of Ti^{4+} and Zr^{4+} substituted Li–Zn ferrites. Indian J. Pure. Appl. Phys. **32**, 193–194 (1994)
24. N.W. Grimes, A.J. Collet, Correlation of infra-red spectra with structural distortions in the spinel series Mg(CrxAl2–x)O4. Phys. Status Solidi (B) **43**, 591–594 (1971)
25. J. Preudhomme, P. Tarte, Spectrochimica Acta part A: molecular spectroscopy. Spectrochim. Acta **27**, 1817–1835 (1971)
26. M.C. Chhantbar, U.N. Trivedi, P.V. Tanna, H.J. Shah, R.P. Vara, H.H. Joshi, K.B. Modi, Infrared spectral studies of Zn-substituted $CuFeCrO_4$ spinel ferrite system. Indian J. Phys. **78** 321–326 (2004)
27. M. Aliahmad, M. Noori, Synthesis and characterization of nickel ferrite nanoparticles by chemical method. Indian J. Phys. **87**, 431–434 (2013)

28. M.M. Rashad, I.A. Ibrahim, A novel approach for synthesis of M-type hexaferrites nanopowders via the co-precipitation method. J. Mater. Sci. **22**, 1796–1803 (2011)
29. T.R. Wagner, Preparation and Crystal Structure Analysis of Magnetoplumbite-Type $BaGa_{12}O_{19}$. J. Solid State Chem. **136**, 120–124 (1998)
30. C. Singh, S. Bindra Narang, I.S. Hudiara, Y. Bai, F. Tabatabaei, Static magnetic properties of Co and Ru substituted Ba–Sr ferrite. Mater. Res. Bull. **43**, 176–184 (2008)
31. M.T. Rahman, M. Vargas, C.V. Ramana, Structural characteristics, electrical conduction and dielectric properties of gadolinium substituted cobalt ferrite. J. Alloys Comp. **617**, 547–562 (2014)
32. B. Wang, J. Wei, Y. Yang, T. Wang, F. Li, Investigation on peak frequency of the microwave absorption for carbonyl iron/epoxy resin composite. J. Magn. Magn. Mater. **323** 1101–1103 (2011)
33. N.-N. Song, Y.J. Ke, H.-T. Yang, H. Zhang, X.-Q. Zhang, B.-G. Shen, Z.-H. Cheng, Integrating giant microwave absorption with magnetic refrigeration in one multifunctional intermetallic compound of $LaFe_{11.6}Si_{1.4}C_{0.2}H_{1.7}$. Sci. Rep. **2291**, 1–5 (2013)
34. A.M. Nicolson, G.F. Ross, Measurement of the intrinsic properties of materials by time-domain techniques. IEEE Trans. Instrum. Meas. **19**, 377–382 (1970)
35. T. Inui, K. Konishi, K. Oda, Fabrications of broad-band RF-absorber composed of planar hexagonal ferrites. IEEE Trans. Magn. **35**, 3148–3150 (1999)
36. P.T. Tho, C.T.A. Xuan, D.M. Quang, T.N. Bach, T.D. Thanh, N.T.H. Le, D.H. Manh, N.X. Phuc, D.N.H. Nam, Microwave absorption properties of dielectric $La_{1.5}Sr_{0.5}NiO_4$ ultrafine particles. Mater. Sci. Eng. **186**, 101–105 (2014)